Model of a Micromechanical Accelerometer Based on the Phenomenon of Modal Localization

Vasilisa Igumnova(✉), Lev Shtukin, Alexey Lukin, and Ivan Popov

Peter the Great St. Petersburg Polytechnic University (SPbPU), Saint Petersburg, Russia
igumnova_vs@spbstu.ru

Abstract. In the present work, a model of a microelectromechanical accelerometer with two movable beam elements located between two stationary electrodes is proposed. The action of portable inertia forces in the longitudinal direction leads to a change in the spectral properties of the system, which is a useful output signal of the sensor. The dynamics of the system in the presence of a weak electrostatic coupling between the sensitive elements is characterized by the phenomenon of modal localization - a significant change in the amplitude relationships for the forms of in-phase and antiphase oscillations with small changes in the measured component of the object's acceleration vector. The diagrams of the equilibrium positions and the dependences of the natural frequency are constructed with varying the potential difference V and ΔV. The dependences of the frequencies and the ratio of the components of the eigenvector on the external disturbance are investigated. It is shown that the sensitivity of a sensor based on modal localization can be orders of magnitude higher than the sensitivity of known systems based on measuring the shift of natural frequencies.

Keywords: Resonant accelerometer · Weakly coupled system · Modal localization

1 Introduction

Currently, micro-electromechanical systems (MEMS) are widely used in various technical applications, as well as for the study of fundamental physical phenomena. In weakly coupled resonators, the phenomenon of modal localization of oscillations is known. The mode localization phenomenon is defined as the limitation of the vibration energy of one element of a coupled system when disturbances appear in the system in the form of a change in the rigidity of the structure. Another phenomenon of coupled systems in which mode localization is manifested is a change in the eigenvalue curve [7]. Veering occurs when the frequencies of the two modes approach and deviate from each other when the

D. A. Indeitsev and A. M. Krivtsov (Eds.): APM 2020, LNME, pp. 159–171, 2022.
https://doi.org/10.1007/978-3-030-92144-6_12

external control parameter changes. The sensitivity of sensors in which mode localization is implemented can be 1–4 orders of magnitude higher than that of sensors based on measuring the frequency shift [1,2], that is, it becomes possible to create ultra-high sensitivity sensors. Also, sensors of this type, to a small extent with respect to sensors based on the measurement of frequency shift, are sensitive to environmental factors: temperature, pressure, etc. In work [3], various approaches are presented for increasing the sensitivity of the resonator for sensory applications. An analytical and numerical study of a MEMS resonance accelerometer is presented in [4]. The use of weakly coupled systems that implement the modal localization phenomenon increases the sensitivity of the sensor by orders of magnitude compared to the sensitivity of a sensor with a single resonator. A review of the use of such MEMS resonators is given in [5]. The article [6] describes a resonant accelerometer with four degrees of freedom, which has an electromechanical weak coupling. This makes it possible to achieve high sensor sensitivity over a wide range of acceleration measurements. In [8], a theoretical and experimental study was made of the phenomenon of mode localization for both mechanically and electrically coupled two microbeams. In addition to studying the problem of eigenvalues and the effect of lateral electrode displacement on the position of the pivot point, it was found that a decrease in damping at one of the resonators of a coupled system can lead to an increase in the quality factor of the system.

In this work, we study the dynamics of a resonant accelerometer, consisting of two beam elastic elements located between two stationary electrodes (Fig. 1).

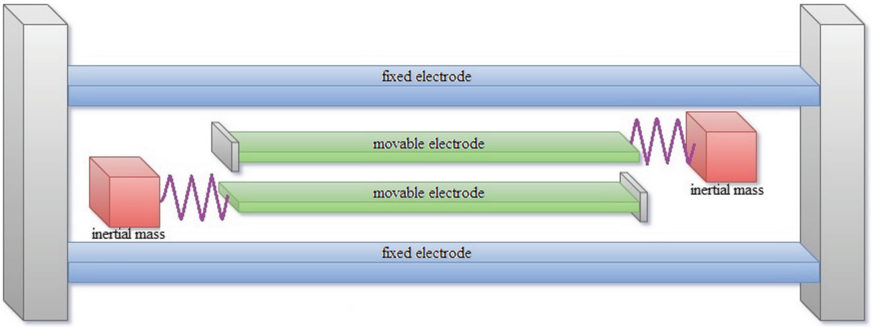

Fig. 1. Scheme accelerometer

When acceleration occurs in the system, inertial masses move, which in turn creates a longitudinal compressive force for one resonator and a tensile force for the other resonator. The action of portable inertia forces in the longitudinal direction leads to a change in the spectral properties of the system. As shown below, in the presence of a weak electrostatic coupling between the sensitive elements, the dynamics of the system is characterized by the phenomenon of modal localization - a significant change in the amplitude relationships for the

forms of in-phase and antiphase oscillations with small changes in the measured component of the object's acceleration vector.

2 Derivation of the Equations of Motion

The equations of motion of the first and second inertial mass (IM), respectively:

$$\begin{cases} -M\ddot{y_1} - cy_1 - c(y_1 - u_1(l)) - MW = 0, \\ M\ddot{y_2} + cy_2 + c(y_2 - u_2(l)) - MW = 0, \end{cases} \tag{1}$$

where y_1, y_2 - longitudinal movement of the first and second IM, respectively, M - mass, c - spring stiffness, W - hull acceleration, $u_1(l), u_2(l)$ - displacement of the end of the first and second beam element.

Neglecting relative acceleration, we can obtain the law of motion of the first and second MI, respectively:

$$\begin{cases} y_1 = \frac{1}{2c}(cu_1(l) - MW), \\ y_2 = \frac{1}{2c}(cu_2(l) + MW). \end{cases} \tag{2}$$

The equation of longitudinal vibrations has the form:

$$m\ddot{u} - ESu'' = ES(\frac{1}{2}w'^2 - u'w'^2)' + EI[w'(w''' - u'''w' - 2u''w'' - 3u'w''')]', \tag{3}$$

where u - longitudinal displacements of the beam, w - transverse displacements, m - mass of the beam, E - Young's modulus, S - cross-sectional area, I - moment of inertia. The term $\frac{1}{2}w'^2$ associated with elastic restorative force.

Neglecting the dynamics and small terms, we obtain a simplified equation of longitudinal vibrations with the corresponding boundary conditions:

$$ES(u'' + (\frac{1}{2}w'^2)) = 0, \tag{4}$$

$$u(0) = 0, \qquad N(l) = c[u(l) - y], \tag{5}$$

where $N(l)$ - longitudinal force in the end section. The axial inertial forces of the beam are not taken into account, therefore, the longitudinal force is constant along the entire length of the beam.

Expressions for longitudinal forces N_1 and N_2 will be of the form:

$$\begin{cases} N_1 = \frac{1}{2}[MW - \frac{1}{2}c\int\limits_0^l w_1'^2 dx], \\ N_2 = \frac{1}{2}[-MW - \frac{1}{2}c\int\limits_0^l w_2'^2 dx]. \end{cases} \tag{6}$$

Substituting the expressions for N_1 and N_2 in the equation of bending vibrations taking into account electrostatic forces in the interelectrode gaps, we obtain:

$$\begin{cases} EIw_1'''' + c_d\dot{w}_1 + [\frac{1}{2}MW - \frac{1}{4}c\int\limits_0^l w_1'^2 dx]w_1'' + \rho S\ddot{w}_1 - \frac{1}{2}\frac{\varepsilon_0 bV^2}{(d-w_1)^2} \\ \qquad + \frac{1}{2}\frac{\varepsilon_0 b\Delta V^2}{(d+w_1-w_2)^2} = 0, \\ EIw_2'''' + c_d\dot{w}_2 + [-\frac{1}{2}MW - \frac{1}{4}c\int\limits_0^l w_2'^2 dx]w_2'' + \rho S\ddot{w}_2 + \frac{1}{2}\frac{\varepsilon_0 bV^2}{(d+w_2)^2} \\ \qquad - \frac{1}{2}\frac{\varepsilon_0 b\Delta V^2}{(d+w_1-w_2)^2} = 0. \end{cases} \tag{7}$$

where ε_0 - is the dielectric constant of the gap medium, b - beam width, V - voltage between the stationary electrode and the beam, ΔV - voltage between two beam elements.

Model Parameters:

Table 1. System parameters

Parameter	Value	Parameter	Value
Beam length (l)	600 μm	Air gap (d)	3 μm
Beam width (b)	120 μm	Spring stiffness (c)	65.4 N/m
Beam thickness (h)	3 μm	Mass of the weight (M)	5.02e–9 kg
Young's modulus of silicon (E)	109 GPa	Silicon Density (ρ)	2328 kg/m^3
Dielectric permittivity (ε)	1	Dielectric constant (ε_0)	8.85e–12 F/m

Enter dimensionless parameters:

$$C_{non} = \frac{12c_d l^4}{ETbh^3}, \qquad C_{sp} = \frac{3cd^2 l}{Ebh^3}, \qquad P_{non} = \frac{6MWl^2}{Ebh^3}, \qquad \alpha = \frac{6\varepsilon_0 l^4}{Eh^3 d^3}. \tag{8}$$

$$w_1 = \tilde{w}_1 d, \qquad w_2 = \tilde{w}_2 d, \qquad x = \tilde{x}l, \qquad t = \tilde{t}T, \qquad T = \sqrt{\frac{\rho S l^4}{ET}}. \tag{9}$$

Omitting the sign $\sim$, we obtain the system of equations in the dimensionless form:

$$\begin{cases} w_1'''' + C_{non}\dot{w}_1 + \ddot{w}_1 + [P_{non} - C_{sp}\int\limits_0^1 w_1'^2 dx]w_1'' - \frac{\alpha V^2}{(1-w_1)^2} + \frac{\alpha\Delta V^2}{(1+w_1-w_2)^2} = 0, \\ w_2'''' + C_{non}\dot{w}_2 + \ddot{w}_2 + [-P_{non} - C_{sp}\int\limits_0^1 w_2'^2 dx]w_2'' + \frac{\alpha V^2}{(1+w_2)^2} - \frac{\alpha\Delta V^2}{(1+w_1-w_2)^2} = 0. \end{cases} \tag{10}$$

3 Finding Static Deflections

We study the dependence of the equilibrium position of the system on the strength of the electric field. The first Eq. (10) is multiplied by the denominator $(1 - w_1)^2(1 + w_1 - w_2)^2$, and the second equation is multiplied by

$(1 + w_2)^2(1 + w_1 - w_2)^2$ and apply the Galerkin method in the expansion in its own forms of an articulated beam:

$$w_1(x,t) = \sum_{i=1}^{n} C_i(t)\phi_i(x), \qquad w_2(x,t) = \sum_{i=1}^{n} D_i(t)\phi_i(x). \tag{11}$$

Nonlinear equations of statics will look like:

$$\begin{cases} \int\limits_0^1 \phi_j \sum\limits_{i=1}^{n} C_i\phi_i''''dx + P_{non}\int\limits_0^1 \phi_j \sum\limits_{i=1}^{n} C_i\phi_i''dx - C_{sp}\int\limits_0^1 \sum\limits_{i=1}^{n} C_i\phi_i'^2 dx \int\limits_0^1 \phi_j \sum\limits_{i=1}^{n} C_i\phi_i''dx \\ \qquad - \int\limits_0^1 \phi_j \frac{\alpha V^2}{(1 - \sum\limits_{i=1}^{n} C_i\phi_i)^2} + \int\limits_0^1 \phi_j \frac{\alpha \Delta V^2}{(1 + \sum\limits_{i=1}^{n} C_i\phi_i - \sum\limits_{i=1}^{n} D_i\phi_i)^2} = 0, \\ \int\limits_0^1 \phi_j \sum\limits_{i=1}^{n} D_i\phi_i''''dx - P_{non}\int\limits_0^1 \phi_j \sum\limits_{i=1}^{n} D_i\phi_i''dx - C_{sp}\int\limits_0^1 \sum\limits_{i=1}^{n} D_i\phi_i'^2 dx \int\limits_0^1 \phi_j \sum\limits_{i=1}^{n} D_i\phi_i''dx \\ \qquad + \int\limits_0^1 \phi_j \frac{\alpha V^2}{(1 + \sum\limits_{i=1}^{n} D_i\phi_i)^2} - \int\limits_0^1 \phi_j \frac{\alpha \Delta V^2}{(1 + \sum\limits_{i=1}^{n} C_i\phi_i - \sum\limits_{i=1}^{n} D_i\phi_i)^2} = 0. \end{cases} \tag{12}$$

Figure 2 shows diagrams of equilibrium positions depending on the potential differences V and ΔV. The solid line indicates stable equilibrium position, and the dashed line indicates unstable.

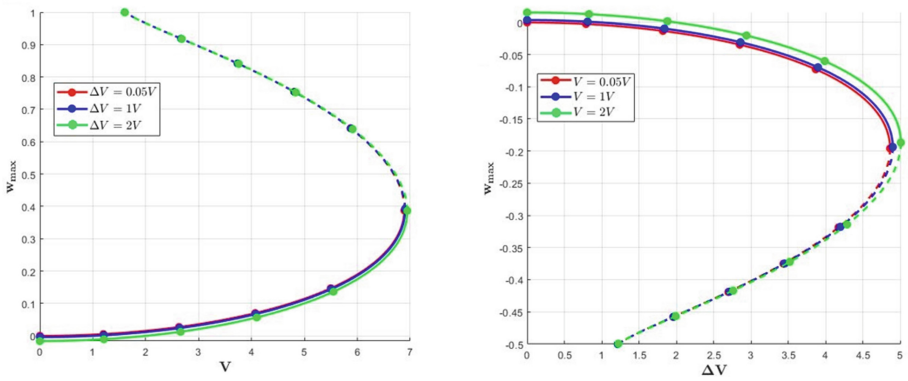

Fig. 2. Deflection in the middle of the upper beam from potential differences V and ΔV.

For greater clarity of the results, Fig. 3 shows a bifurcation diagram of the equilibrium positions in 3D with varying parameters.

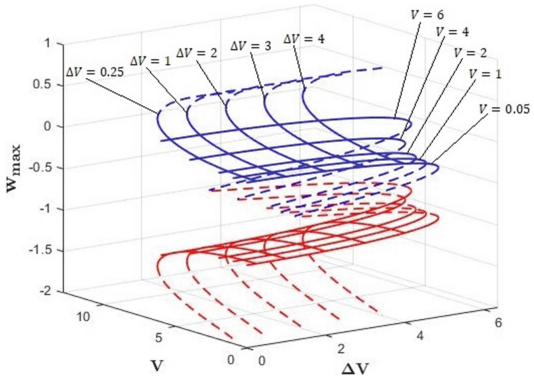

Fig. 3. Equilibrium diagram for various values of V and ΔV. Blue shows the deflection for the upper beam, red - the deflection of the lower beam.

4 Comparison of Equilibrium Diagrams for Two Models

If we initially assume that the field is concentrated in the middle of the beam, then Eqs. (10) will have the form:

$$\begin{cases} w_1'''' + C_{non}\dot{w}_1 + \ddot{w}_1 + [P_{non} - C_{sp}\int\limits_0^1 w_1'^2 dx]w_1'' - \frac{\alpha V^2 \delta(x-\frac{1}{2})}{(1-w_1)^2} + \frac{\alpha \Delta V^2 \delta(x-\frac{1}{2})}{(1+w_1-w_2)^2} = 0, \\ w_2'''' + C_{non}\dot{w}_2 + \ddot{w}_2 + [-P_{non} - C_{sp}\int\limits_0^1 w_2'^2 dx]w_2'' + \frac{\alpha V^2 \delta(x-\frac{1}{2})}{(1+w_2)^2} - \frac{\alpha \Delta V^2 \delta(x-\frac{1}{2})}{(1+w_1-w_2)^2} = 0. \end{cases} \tag{13}$$

We apply the Galerkin method to Eq. (13), leaving one form in the expansion:

$$w_1(x,t) = q_1(t)\phi_1(x), \qquad w_2(x,t) = q_2(t)\phi_1(x). \tag{14}$$

System of equations can be obtained:

$$\begin{cases} \ddot{q_1} + (97.4 - 9.87P_{non})q_1 + 48.7C_{sp}q_1^3 - \frac{2\alpha V^2}{(1-q_1)^2} + \frac{2\alpha \Delta V^2}{(1+q_1-q_2)^2} = 0, \\ \ddot{q_2} + (97.4 + 9.87P_{non})q_2 + 48.7C_{sp}q_2^3 + \frac{2\alpha V^2}{(1+q_2)^2} - \frac{2\alpha \Delta V^2}{(1+q_1-q_2)^2} = 0. \end{cases} \tag{15}$$

The bifurcation diagram for the exact and approximate equations has the form:

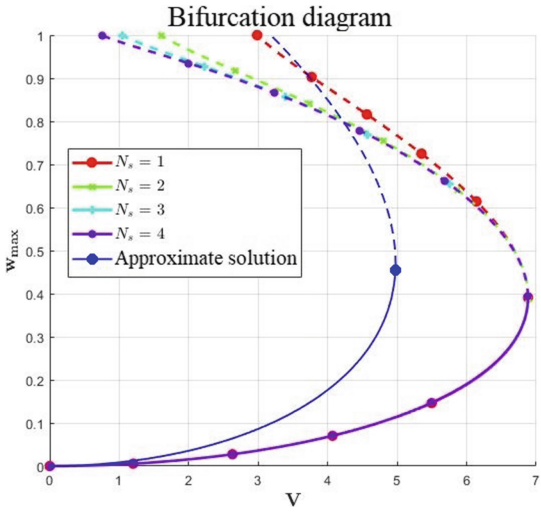

Fig. 4. Comparison of equilibrium diagrams

From Fig. 4 it can be seen that the exact and approximate solutions have a similar form of the bifurcation curve, but have differences in the value of the voltage corresponding to the "pull-in" effect. It is also seen that as the number of terms in the expansion increases, the solution approaches the exact one.

5 Analysis of the Spectral Properties of the System

Let us return to the system of equations in the dimensionless form:

$$\begin{cases} w_1'''' + C_{non}\dot{w}_1 + \ddot{w}_1 + [P_{non} - C_{sp}\int\limits_0^1 w_1'^2 dx]w_1'' - \frac{\alpha V^2}{(1-w_1)^2} \\ \qquad + \frac{\alpha \Delta V^2}{(1+w_1-w_2)^2} = 0, \\ w_2'''' + C_{non}\dot{w}_2 + \ddot{w}_2 + [-P_{non} - C_{sp}\int\limits_0^1 w_2'^2 dx]w_2'' + \frac{\alpha V^2}{(1+w_2)^2} \\ \qquad - \frac{\alpha \Delta V^2}{(1+w_1-w_2)^2} = 0. \end{cases} \tag{16}$$

Next, we decompose the deflections of the beam elements into a static and dynamic part:

$$w_1(x,t) = w_{1s}(x) + w_{1d}(x,t), \qquad w_2(x,t) = w_{2s}(x) + w_{2d}(x,t). \tag{17}$$

where $w_{1s}(x)$ and $w_{2s}(x)$ are the result of solving the static problem. We obtain the equations for the dynamic component:

$$\begin{cases} w''''_{1d} + C_{non}\dot{w}_{1d} + \ddot{w}_{1d} + [P_{non} - C_{sp}\int\limits_0^1 w'^2_{1d}dx]w''_{1d} \\ \qquad + \frac{2\alpha V^2}{(1-w_{1s})^3} + \frac{2\alpha\Delta V^2}{(1+w_{1s}-w_{2s})^3}(w_{2d} - w_{1d}) = 0, \\ w''''_{2d} + C_{non}\dot{w}_{2d} + \ddot{w}_{2d} + [-P_{non} - C_{sp}\int\limits_0^1 w'^2_{2d}dx]w''_{2d} \\ \qquad - \frac{2\alpha V^2}{(1+w_{2s})^3} - \frac{2\alpha\Delta V^2}{(1+w_{1s}-w_{2s})^3}(w_{2d} - w_{1d}) = 0. \end{cases} \tag{18}$$

For the analysis of free vibrations, we also apply the Galerkin method, taking into account only the lower vibration modes of two beams:

$$w_{1d}(x,t) = u_1(t)\phi_1(x), \qquad w_{2d}(x,t) = v_1(t)\phi_1(x). \tag{19}$$

The equations of motion in matrix form can be written as:

$$M\ddot{U} + C\dot{U} + KU = 0, \tag{20}$$

where $M = \begin{pmatrix} 1 & 0 \\ 0 & 1 \end{pmatrix}$ - mass matrix, $C = \begin{pmatrix} C_{non} & 0 \\ 0 & C_{non} \end{pmatrix}$ - dissipation matrix (further consider $C = 0$), $U = [u_1 \quad v_1]'$ - displacement vector, stiffness matrix:

$$K = \begin{pmatrix} -K_2C_{sp} + K_3V^2 - K_4\Delta V^2 + K_1P_{non} & K_4\Delta V^2 \\ K_4\Delta V^2 & -K_5C_{sp} - K_6V^2 - K_4\Delta V^2 - K_1P_{non} \end{pmatrix}$$

The coefficients of the stiffness matrix has the form:

$$\begin{cases} K_1 = \int\limits_0^1 \phi_1\phi''_1 dx, \quad K_2 = \int\limits_0^1 w'^2_{1s}dx \int\limits_0^1 \phi_1\phi''_1 dx + 2\int\limits_0^1 w'_{1s}\phi'_1 dx \int\limits_0^1 \phi_1 w''_{1s}dx, \\ K_3 = \int\limits_0^1 \frac{2\alpha}{(w_{1s}-1)^3}\phi_1\phi_1 dx, \quad K_4 = \int\limits_0^1 \frac{2\alpha}{(1+w_{1s}-w_{2s})^3}\phi_1\phi_1 dx, \\ K_5 = \int\limits_0^1 w'^2_{2s}dx \int\limits_0^1 \phi_1\phi''_1 dx + 2\int\limits_0^1 w'_{2s}\phi'_1 dx \int\limits_0^1 \phi_1 w''_{2s}dx, \quad K_6 = \int\limits_0^1 \frac{2\alpha}{(w_{2s}+1)^3}\phi_1\phi_1 dx. \end{cases} \tag{21}$$

The eigenfrequencies $\omega_{1,2}$ and the eigenvectors $U_{1,2}$ of the system of Eqs. (21) depend on the dimensionless transport inertia P_{non}. An analysis of the nature of these dependencies allows us to evaluate the sensitivity of the proposed sensor model.

Figure 5 shows the dependence of the natural frequency of the in-phase and antiphase modes with increasing potential differences ΔV and V.

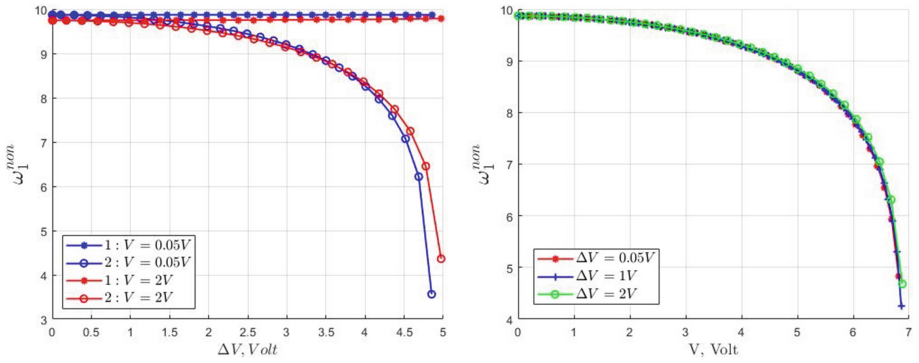

Fig. 5. The dependence of the natural frequency with increasing potential differences ΔV and V.

Let us compare two measurement methods: with a frequency output and with an amplitude output. Figure 6 shows the dependence of the oscillation frequency on the external disturbance.

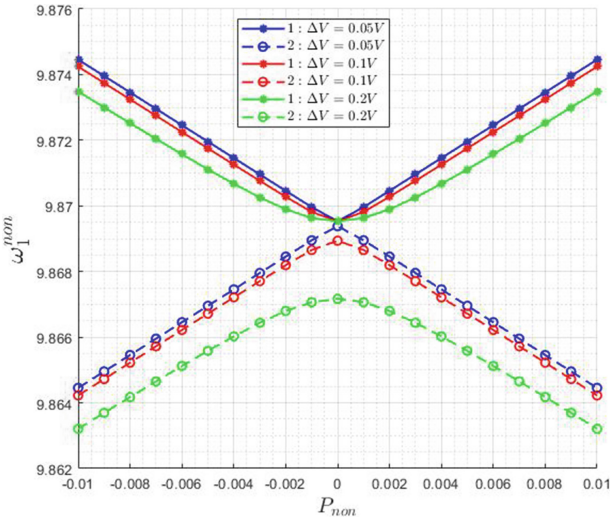

Fig. 6. Dependence of the oscillation frequency on the external disturbance P_{non}. The number "1" indicates the in-phase mode, and the number "2" indicates the antiphase mode. With parameter $V = 0.05V$.

Figure 6 shows the dependence of the frequency on the external disturbance at various ΔV values. It can be seen that with an increase in the weak coupling ΔV, the difference in the frequencies of the in-phase and antiphase modes significantly increases. The region near the value $P_{non} = 0$ is called the veering zone, because,

as can be seen from the figure in this zone, the frequencies of the first and second modes repel each other, but do not intersect in the presence of a small coupling ΔV.

Figure 7 shows the dependence of the oscillation amplitude on the external disturbance.

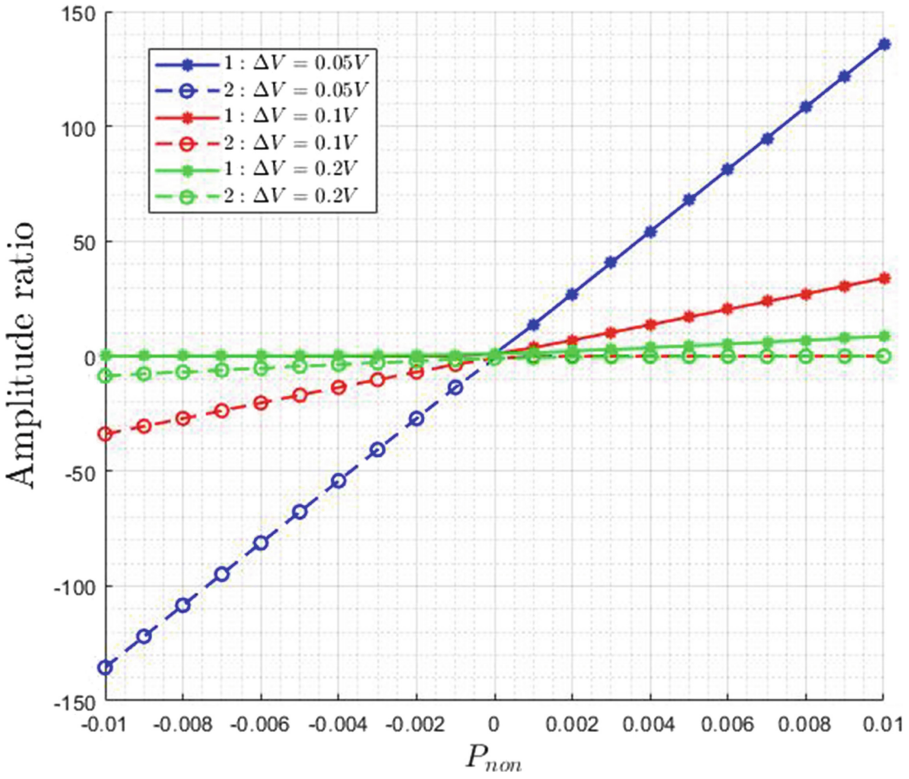

Fig. 7. Dependence of the amplitude of oscillations on the external disturbance P_{non}. The number "1" indicates the in-phase mode, and the number "2" indicates the antiphase mode. With parameter $V = 0.05V$.

Figure 7 shows the dependence of the ratio of the components of the eigenvectors of free vibrations on the external disturbance for various values of ΔV. As can be seen from the figure, with a decrease in the weak coupling ΔV, the dependence of the amplitude indices on external acceleration becomes stronger.

The sensitivity of sensors based on the frequency and based on the amplitude ratio can be calculated by the formulas:

$$S_\omega = |\frac{\omega_i - \omega_i^0}{\omega_i^0}|, \qquad S_\alpha = |\frac{u_i - u_i^0}{u_i^0}|, \tag{22}$$

where ω_i^0 and u_i^0 are the eigenfrequency and amplitude ratio of the components of the eigenvector in the absence of weak coupling, that is, $\Delta V = 0$, $i = 1, 2$ denotes the first mode (in-phase) and the second mode (antiphase), respectively.

Figure 8 and Fig. 9 show the dependences of the parameters S_ω and S_α on the dimensionless axial component of the acceleration P_{non}.

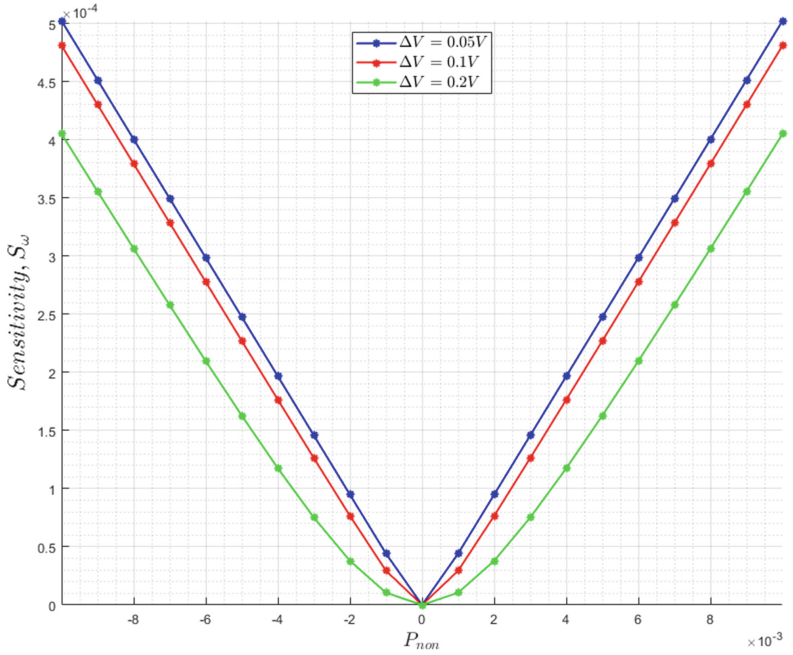

Fig. 8. The sensitivity of the sensor based on the frequency from the external disturbance P_{non}. With $V = 1V$.

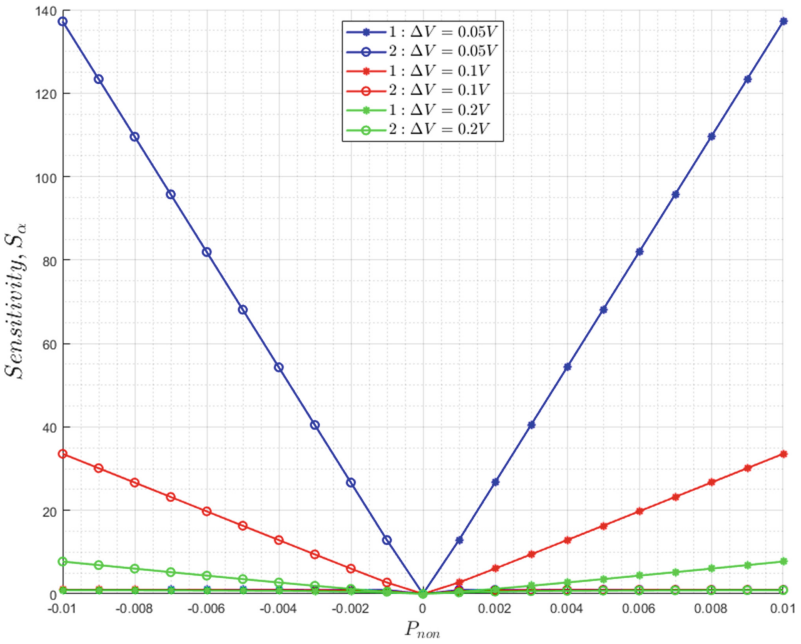

Fig. 9. Sensitivity of a sensor based on modal localization from the external disturbance P_{non}. The number "1" indicates the in-phase mode and the number "2" indicates the antiphase mode. With parameter $V = 1V$.

As can be seen from the figures, the sensitivity of the accelerometer using the principle of localization of oscillations is several orders of magnitude higher than in a sensor with a frequency output.

6 Conclusions

In the present work, a model of a microelectromechanical accelerometer with two movable beam elements located between two stationary electrodes is proposed. The diagrams of the equilibrium positions and the dependences of the natural frequency are constructed with varying the potential difference V and ΔV. The dependences of the frequencies and the ratio of the components of the eigenvector on the external disturbance are investigated. It is shown that the sensitivity of a sensor based on the phenomenon of localization of oscillations in weakly coupled systems can be orders of magnitude higher than the sensitivity of the system in the mode of measuring the shift in natural frequencies. The symmetry of the proposed sensor architecture also ensures its high resistance to environmental changes (temperature disturbances, pressure changes).

The work was supported by the RFBR grant 20-01-00537.

References

1. Zhao, C., Wood, G.S., Xie, J., Chang, H., Pu, S.H., Kraft, M.: A three degree-of-freedom weakly coupled resonator sensor With enhanced stiffness sensitivity. J. Microelectromech. Syst. **25**(1), 38–51 (2016)
2. Manav, M., Phani, A.S., Cretu, E.: Mode localization and sensitivity in weakly coupled resonators. IEEE Sensors J. **19**(8), 2999–3007 (2018)
3. Hajjaj, A.Z., Jaber, N., Ilyas, S., Alfosail, F.K., Younis, M.I.: Linear and nonlinear dynamics of micro and nano-resonators: review of recent advances. Int. J. Non-Linear Mech. (2019)
4. Zhang, H., Kraft, M.: An acceleration sensing method based on the mode localization of weakly coupled resonators (2017)
5. Zhao, C., Montaseri, M.H., Wood, G.S., Pu, S.H., Seshia, A.A., Kraft, M.: A review on MEMS coupled resonators for sensing applications utilizing mode localization. Sens. Actuators, A **249**, 93–111 (2016)
6. Peng, B., Hu, K., Shao, L., Yan, H., Li, L., Wei, X.: A sensitivity tunable accelerometer based on series-parallel electromechanically coupled resonators using mode localization. J. Microelectromech. Syst. **29**(1), 3–13 (2020)
7. Pierre, C., Dowell, E.H.: Localization of vibrations by structural irregularity. J. Sound Vib. **114**(3), 549–564 (1987)
8. Ilyas, S., Younis, M.I.: Theoretical and experimental investigation of mode localization in electrostatically and mechanically coupled microbeam resonators. Int. J. Non-Linear Mech. **125**, 103516 (2020)